


RESEARCH ARTICLE | AUGUST 22 2024

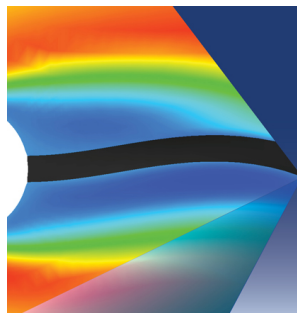
Explicit filtering for large eddy simulation as use of a spectral buffer

Special Collection: [K. R. Sreenivasan: A Tribute on the occasion of his 75th Birthday](#)


Joseph Mathew 

 Check for updates

Physics of Fluids 36, 085181 (2024)
<https://doi.org/10.1063/5.0222335>



Physics of Fluids
Special Topic:
Fluid-Structure Interaction
Guest Editors: A-Man Zhang, Tiegang Liu, Boo Cheong Khoo and Nhan Phan-Thien
[Submit Today!](#)



Explicit filtering for large eddy simulation as use of a spectral buffer

Cite as: Phys. Fluids **36**, 085181 (2024); doi: [10.1063/5.0222335](https://doi.org/10.1063/5.0222335)

Submitted: 7 June 2024 · Accepted: 6 August 2024 ·

Published Online: 22 August 2024



View Online



Export Citation



CrossMark

Joseph Mathew 

AFFILIATIONS

Department of Aerospace Engineering, Indian Institute of Science, Bangalore 560012, India

Note: This paper is part of the special topic, K. R. Sreenivasan: A Tribute on the occasion of his 75th Birthday.

^{a)} Author to whom correspondence should be addressed: joseph@iisc.ac.in

ABSTRACT

The explicit filtering method for large eddy simulation (LES), which comprises integration of the governing equations without any added terms for sub-grid-scale modeling, and the application of a low-pass filter to transported fields, is discussed. The shapes of filter response functions of numerical schemes for spatial derivatives and the explicit filter that have been used for several LES are examined. Generally, these are flat (no filtering) over a range of low wavenumbers and then fall off over a small range of the highest represented wavenumbers. It is argued that this high wavenumber part can be viewed as a spectral buffer analogous to physical buffer (or sponge) zones used near outflow boundaries. With grid refinement, this buffer moves to higher wavenumbers and solutions are obtained with little change over a range of low wavenumbers but with added, correct, high wavenumber content. Examples show LES solutions to converge toward direct numerical simulations monotonically. Connections to other widely used methods are also explained.

Published under an exclusive license by AIP Publishing. <https://doi.org/10.1063/5.0222335>

I. INTRODUCTION

Large eddy simulation (LES) connotes a numerical simulation that is restricted to a range of the largest scales of a turbulent flow. The approximation is useful when the solution is qualitatively correct, and typical quantities of interest, such as flow statistics, are obtained with acceptable accuracy. The error is acceptable because of the great reduction in computing effort (grid size and computation time) compared with that required for a direct numerical simulation (DNS) that contains the full range of dynamically significant scales. Many techniques, both turbulence models and numerical methods, have been proposed to address shortcomings revealed as LES began to be applied to wider classes of problems. A comprehensive presentation of techniques and sample results can be found in Sagaut.¹ Much of the effort had been directed at finding the best sub-grid-scale (SGS) model, which must capture the effect of the omitted small scales on the computed large scales. It cannot be said that any one approach has emerged as a sole best method. Instead, practitioners adopt a particular method (numerical scheme and SGS model), which has proved successful for their studies, whose requirements for each class of flows (free shear flows and wall-bounded flows) are known from experience. This paper discusses some aspects of an explicit filtering approach, introduced in Mathew *et al.*,² that have since become clearer from its application to a variety of problems.

In the literature, explicit filtering can also refer to filtering nonlinear terms alone as proposed by Lund³ to control numerical error; notably, it was not an SGS model. Moreover, a response to reading about steps in the explicit filtering method considered here has been to conclude that it is a procedure for “cleaning” small scales, or that it is for de-aliasing. To emphasize that it is not a part of a numerical method, but is an SGS model, the derivation is repeated below. Further, hereafter this method will be termed EFLES to distinguish from others that incorporate explicit filtering operations. Filtering and filters used in our LES are discussed in Sec. II A, leading to the idea of EFLES as use of a spectral buffer, analogous to physical buffers or sponge regions that have been used, typically, near outflow boundaries. Arguments implied by the shape of the energy spectrum of turbulent flows, that support the use of filters with a flat response function over a range of low wavenumbers, as prescribed by EFLES, follow. Support for these ideas is provided from two examples that show the presence and effects of this buffer at different grid resolutions, filter cutoffs, and Reynolds numbers. Connections to other SGS models are discussed in Sec. IV.

A. Approximate deconvolution model

The explicit filtering method of Mathew *et al.*² was derived from the approximate deconvolution model (ADM).⁴ Salient aspects are

summarized below. Consider the one-dimensional evolution equation for a field $u(x, t)$,

$$\frac{\partial u}{\partial t} + \frac{\partial}{\partial x} f(u) = 0, \tag{1}$$

where $f(u)$ is a nonlinear function. An LES can be interpreted as either obtaining an approximation $\bar{u}(x, t)$ that contains a large scale part of $u(x, t)$, or the approximation that can be obtained on a coarse grid, which implicitly limits the range of wavenumbers in the solution. The LES field is $\bar{u} = G * u = \int G(x - x') u(x') dx'$, where G is a low-pass filter. The evolution equation for $\bar{u}(x, t)$ is obtained by applying the filter to Eq. (1) to get

$$\frac{\partial \bar{u}}{\partial t} + G * \frac{\partial}{\partial x} f(u) = 0. \tag{2}$$

Equation (2) can be written in the form of the original equation with a remainder \mathcal{R} ,

$$\begin{aligned} \frac{\partial \bar{u}}{\partial t} + \frac{\partial}{\partial x} f(\bar{u}) &= \mathcal{R}, \\ \mathcal{R} &= \frac{\partial f(\bar{u})}{\partial x} - G * \frac{\partial f(u)}{\partial x}. \end{aligned} \tag{3}$$

$\mathcal{R} \neq 0$ when $f(u)$ is nonlinear. Since u is not known when solving for \bar{u} , \mathcal{R} must be replaced with a model $\mathcal{R}_m(\bar{u})$ for closure. In ADM,⁴

$$\mathcal{R}_m = \frac{\partial f(\bar{u})}{\partial x} - G * \frac{\partial f(u^*)}{\partial x}, \tag{4}$$

where $u^*(x, t) = Q * \bar{u}$ is an approximation to $u(x, t)$ obtained by the deconvolution of the filtered variable \bar{u} . The equation solved when using ADM is

$$\frac{\partial \bar{u}}{\partial t} + G * \frac{\partial f(Q * \bar{u})}{\partial x} = 0. \tag{5}$$

During the early development of ADM, when the method was applied to different types of problems, filters were obtained from implicit formulas [Padé-type filters $G(x)$, with different values of the filter parameter α .⁵ These filters are discussed in Sec. II A.]. Explicit formulas have also been used.⁶ The *approximate* deconvolution $Q * \bar{u}$ was performed by applying the filter G several times according to an expansion of the operator Q in terms of G . In all cases, excellent results for LES were presented. Around the same time, Geurts⁷ examined a similar de-filtering, taking the primary filter to be a top-hat function in physical space and inversion to be exact for polynomials. It was not understood whether there was a best convolution–deconvolution pair G and Q , or that all pairs that satisfied some property would be suitable. As will be shown below, the derivation of EFLES revealed that the solution depends on the effective filter $E = Q * G$ only, rather than independently on both a filter G and a deconvolution operator Q .

B. Explicit filtering implementation of ADM

The implementation of ADM by solving Eq. (5) involves the following steps to obtain $\bar{u}(x, t^{n+1})$ at the $n + 1$ time step given $\bar{u}(x, t^n)$:

1. Deconvolution: $u^* = Q * \bar{u}(x, t^n)$.
2. Integration of Eq. (5): $\bar{u}(x, t^n) \rightarrow \bar{u}(x, t^{n+1})$.

This integration step by the Euler forward formula is

$$\bar{u}(x, t^{n+1}) = \bar{u}(x, t^n) - \Delta t G * \frac{\partial f(u^*)}{\partial x}$$

and can be evaluated in two steps,

$$a(x) = u^*(x, t^n) - \Delta t \frac{\partial f(u^*)}{\partial x}, \tag{6}$$

$$\bar{u}(x, t^{n+1}) = G * a(x) + [\bar{u}(x, t^n) - G * u^*(x, t^n)]. \tag{7}$$

The quantity within the square brackets in Eq. (7) is small and can be neglected, because the essential requirement for the deconvolved field is that $u^* \approx u$ over a range of large scales; then, $\bar{u} = G * u \approx G * u^*$. The intermediate field $a(x)$ can also be written as $u^*(x, t^{n+1})$. This alternate implementation comprises the following three steps:

1. Deconvolution: $u^*(x, t^n) = Q * \bar{u}(x, t^n)$.
2. Integration of Eq. (1) with u^* instead of u : $u^*(x, t^n) \rightarrow u^*(x, t^{n+1})$ [evaluating $a(x)$ of Eq. (6)].
3. Filtering: $\bar{u}(x, t^{n+1}) = G * u^*(x, t^{n+1})$ [Eq. (7)].

Mathew *et al.*² observed that, in this latter form, the simulation proceeds by repeating the following two steps: an integration of the original evolution Eq. (1), followed by filtering and deconvolution that can be combined into an (explicit) filtering of the evolving field with a resultant filter $E = G * Q$ (step 3 of a time step is combined with step 1 of the following time step). Since Q is an approximate inverse of G over a range of large scales, by definition, $E \approx I$ over that range of large scales. Beyond that range, we shall require E to filter out content.

In ADM [Eq. (5)], operators G and Q , and their parameters, were assumed, and an estimate u^* was found. Thus, it is a structural model closure for SGS Sagaut.¹ Although it is a procedure and not obtained by adding terms for SGS closure, it is nevertheless an SGS model. It is not a procedure to provide stability for a numerical scheme, or to clean up small scales. However, ADM provided no guidelines on what G ought to be, and different operators Q could be obtained for the same G . Another criticism was that ADM does not account explicitly for the effect of small scales omitted from the computation because the operator Q only amplifies content within the represented range of scales—the estimate u^* has no dependence on the small scales that are not computed. In Sec. II B 1, it is argued why such effects are not significant. The derivation of the explicit filtering method for implementing ADM revealed a *principle* for LES: *a structural SGS model for LES is realized by integrating the governing equations without adding any model terms and applying a flat, low-pass filter to the transported variables after every time step; consistently, discretization formulas for spatial operations must be high-resolution ones that have little error over a range of large scales.*

II. EFLES FOR TURBULENT FLOW

For LES of a turbulent flow, the model Eq. (1) is replaced by the Navier–Stokes equations. For incompressible flow, the steps at each time step comprise integrating the momentum equation to obtain a velocity field, solving a Poisson equation for the pressure field, and correcting the velocity field to be divergence-free as for a DNS. Additionally, an explicit filter E should be applied to this velocity field. Since these are three-dimensional fields, spatial filters E should be applied in the three directions. For compressible flow, there are two other transport equations for, say, density and energy, and these fields would also be filtered after every time step. Other fields, like

temperature or pressure, that appear in the equations need not be filtered; their spectral content gets limited by their dependence on transported fields, even if, in a single step, nonlinear relations like the equation of state extend their spectral range. Incidentally, it is not necessary to use filters that commute with differentiation, since commutation is not invoked at any stage in deriving this method.

When the momentum equation is written in terms of the LES velocity, $\mathbf{u}(\mathbf{x}, t)$, the remainder \mathcal{R} is termed the SGS stress, which requires an SGS model. SGS modeling can be classified broadly into structural and functional models.¹ A structural model is obtained by replacing the full-spectrum fields in SGS terms with an approximation obtained from the computable partial spectrum fields. ADM is an example that replaces the velocity field $\mathbf{u}(\mathbf{x}, t)$ with the approximation $\mathbf{u}^*(\mathbf{x}, t)$ that has been obtained by the deconvolution of the LES field $\bar{\mathbf{u}}(\mathbf{x}, t)$. A velocity estimation model is another kind where an approximation to $\mathbf{u}(\mathbf{x}, t)$ is obtained by an integration of the governing equations (or an approximation that makes computations economical) with a slightly larger spectral content and for short durations.⁸ An example of a functional model is the Smagorinsky model. A well-known feature of turbulent flow is the net transfer of energy from larger scales to smaller scales where most of the viscous occurs. In an LES, only a large scale part of the flow is computed, and dissipation scales are not present. Although energy cascades down to the smallest computed scales, since physical dissipation is insufficient, we observe energy growth at high wavenumbers in the form of wiggles in the solution in physical space; soon the solution will diverge unless an SGS model is employed. An SGS model that prevents this growth of high wavenumber content is a functional model. The Smagorinsky model dissipates spectral content at all scales but increasingly at the highest wavenumbers and is thus a functional model. By dissipating in the computed scale range itself, solution divergence is prevented. The coefficient of the model term controls the magnitude of dissipation, and when it is determined dynamically from the evolving fields themselves,⁹ the model has been found to be more generally useful, since the analyst does not need to specify a flow-dependent coefficient. Although EFLES was derived as a structural model, it also serves as a functional model—to be explained below after discussing filters.

A large number of studies have appeared that use the AFRL-FDL3DI code, which combines an explicit filtering step with high-resolution, compact difference schemes. The method was first described in Visbal and Gaitonde.¹⁰ Examples of LES were reported subsequently.^{11,12} Derivatives were computed with fourth and sixth-order compact differences, and conserved variables were filtered with eighth and tenth-order Padé filters; there were no added SGS model terms in the equations that were solved. The numerical scheme and the explicit filter have flat response functions with a smooth falloff near the high wavenumber end. Bogey and Bailly¹³ proposed high-order explicit difference schemes (eighth-, tenth-, and 12th-order) with optimized coefficients that have good resolution characteristics like compact schemes. They also devised a selective filter with response functions similar to that shown in Fig. 1 (see Fig. 3 in their paper¹³). They have used this method for LES of round jets and computed turbulence profiles and the radiated sound. Both are de facto EFLES methods.

Marinac and Foysi¹⁴ used an optimized sixth-order finite difference scheme for spatial derivatives and an optimized tenth-order explicit filter for their LES for control of aeroacoustics of plane jets. EFLES was applied successfully to a reacting plane jet injected into a

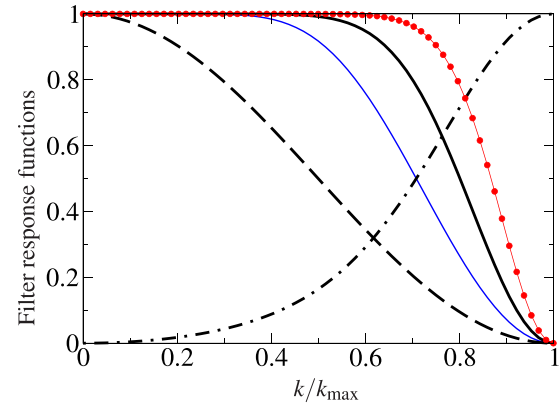


FIG. 1. Filter response functions associated with Padé filter defined by Eq. (8). --: $\hat{G}(k; \alpha = 0)$, - · - · -: $(Q_{ADM}(k) - 1)/J; \alpha = 0, J = 5$, black solid line: $\hat{E}(k; \alpha = 0)$, blue long-dashed line: $\hat{E}(k; \alpha = -0.2)$, and red filled circle with line: $\hat{E}(k; \alpha = 0.2)$.

compressible channel flow.¹⁵ Foysi and Sarkar¹⁶ added a dynamic Smagorinsky term and applied explicit filtering for their LES of round jets in the manner of mixed models; filtering was considered to provide a reconstruction and the Smagorinsky term to provide stabilization. As will be shown in the following, it has been possible to perform LES of compressible round jets without the need for any additional terms.

A. Filter characteristics

Although derived as a structural model, the explicit filtering model of Mathew *et al.*² is a functional model. Before elaborating, let us consider examples of G , Q , and $E = QG$. Let u_j denote values of the function on a uniform grid of N points $x_j = jh$ ($j = 0, 1, \dots, N$). When combined with end point formulas, the following implicit formula provides a filtered field \bar{u}_j :

$$\alpha \bar{u}_{j-1} + \bar{u}_j + \alpha \bar{u}_{j+1} = \left(\alpha + \frac{1}{2} \right) \left(u_j + \frac{1}{2} (u_{j-1} + u_{j+1}) \right). \quad (8)$$

The sole free parameter α controls the shape of the filter response function. We write $\bar{u} = G * u$. For simplicity, suppose u to be periodic, with period 2π . Then, Fourier coefficients of wavenumber k are related as $\hat{\bar{u}}(k) = \hat{G}(k) \hat{u}(k)$, where variables with carets are coefficients of the appropriate Fourier series. Figure 1 shows $\hat{G}(k)$ with $\alpha = 0$. Note that there is significant filtering at all wavenumbers: this filter will distort a function such that high wavenumber content is suppressed and the filtered function will be smoother. Owing to the restriction of the function u to the grid of N intervals, the spectral content of the filtered field is restricted to $0 \leq k \leq k_{\max}$, where $k_{\max} = N/2$. An exact inverse is not possible because content with $k \geq N/2$ is not available. An obvious filter for an approximate inverse is

$$\hat{G}_N^{-1} = \begin{cases} 1/\hat{G} & (0 \leq k < N/2), \\ 0 & (k = N/2). \end{cases}$$

Formally then, the deconvolution filter $Q = G_N^{-1}$. The explicit filter $\hat{E} = \hat{G}Q = 1$ ($0 \leq k < N/2$) and vanishes for $k = N/2$. LES with these filters amounts to integrating the transport equation without any explicit filtering. The explicit filtering SGS model is then inactive and

will prove inadequate, and the code will diverge, *unless* the filtering due to *other* operations, such as numerical differentiation, provides the expected functionality.

The approximate deconvolution operator proposed by Stolz and Adams⁴ is the truncated series,

$$Q_{\text{ADM}} = I + \sum_{j=1}^J (I - G)^j,$$

where I is the identity operator. Figure 1 shows the filter response function for $\hat{Q}_{\text{ADM}}(\alpha = 0)$ when $J = 5$. Also shown are the implied explicit filters $\hat{E} = G\hat{Q}_{\text{ADM}}$ for $\alpha = -0.2, 0, 0.2$. The explicit filter E is flat (*essentially*, no filtering) over a range of low wavenumbers and then falls smoothly to zero over a small part of the highest represented wavenumbers. As α increases, the cutoff wavenumber k_{cutoff} increases. An operational definition of k_{cutoff} could be that $\hat{E}(k_{\text{cutoff}}) = 0.9$.

LES with the AFRL code FDL3DI is like EFLES because the code implements high resolution numerical methods (fourth- or sixth-order compact differences) combined with filters with response functions similar to those in Fig. 1. Examples may be found in Rizzetta *et al.*¹² The difference formulas may be viewed as providing a spectrally accurate derivative combined with low-pass filtering. The implied filter is \bar{k}/k , where $k(k)$ is the modified wavenumber¹⁷ of the difference formula. For symmetric, implicit difference formulas or high-order explicit difference formulas, this implied filter is nearly flat over a range of low wavenumbers and then falls off to zero (see, for example, modified wavenumber formulas in Lele.¹⁷

Chakravorty¹⁸ performed LES of incompressible and variable density (low-Mach number) flows using compact difference formulas. For the staggered grid algorithm, the needed interpolations were also performed using a high-resolution, implicit formula.¹⁹ The implied filters of all numerical procedures were designed to be flat over a range of low wavenumbers and to fall off at high wavenumbers, like the explicit filter E shown in Fig. 1. Five-point stencils were taken and constrained at two or three wavenumbers to design derivative and interpolation formulas with a large range of wavenumbers over which near-spectral accuracy would be obtained. Truncation error was fourth-order for all formulas. The explicit filter, defined on a five-point stencil, has one free parameter and is fourth-order. The filter response functions for the explicit filter, the implied filters for the first derivative, and interpolation are shown in Fig. 2. Note that there is a clear separation between the cutoff wavenumbers of procedures in the numerical scheme and the explicit filter. The cutoff is at a smaller wavenumber for the explicit filter ($k_{\text{cutoff}} \approx 0.7k_{\text{max}}$). Below the cutoff, spectral accuracy is maintained. A similar relation between cutoffs of explicit filter and numerical scheme was used in Mathew *et al.*² for LES of supersonic channel flow.

The earlier papers^{2,20} had advocated that the cutoff wavenumber of the explicit filter should be smaller than that of the numerical method. The operations in Chakravorty¹⁸ have also followed this principle. However, it is not necessary because it is the combination that is effective in a simulation. For the LES of Visbal and Rizzetta,¹¹ when the tenth-order filter is applied with a high value for the filter parameter of 0.49, the cutoff of the filter is very close to the maximum wavenumber and clearly larger than that of the derivative operations. We have a similar experience in other LES. Figure 3 shows response functions of the implied filter of the standard sixth-order compact difference formula [Eq. (2.1.7) in Lele¹⁷] and a tenth-order Padé filter (filter F10 in Table

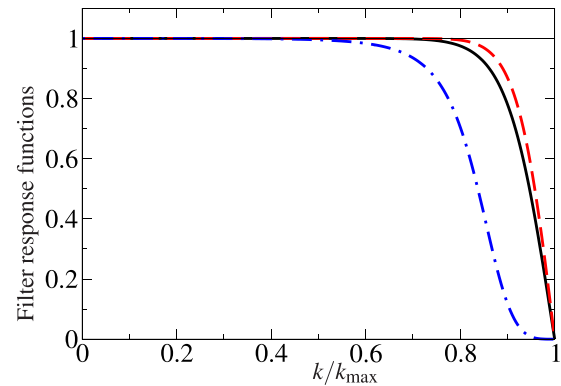


FIG. 2. Filtering of formulas designed by Chakravorty.¹⁸ —: first derivative; red dashed line: interpolation; and blue dotted-dashed line: explicit filter E .

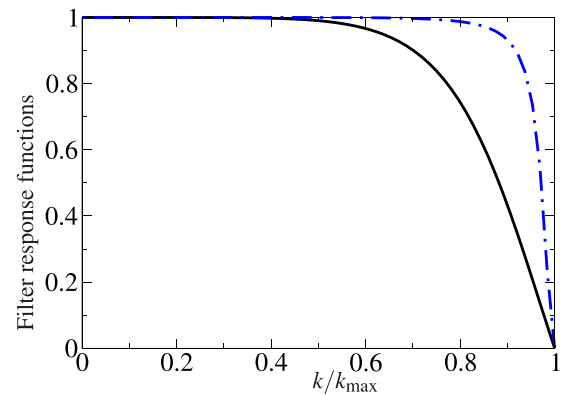


FIG. 3. Filtering of standard sixth-order compact difference formula (—) and tenth-order filter F10 with $\alpha = 0.498$ (blue dotted-dashed line).

IV of Visbal and Rizzetta¹¹ with parameter $\alpha = 0.498$). The implied filter of the difference formula has a smaller cutoff than the optimized schemes shown in Fig. 2. So it has been sufficient to use an explicit filter with a higher cutoff than that of the difference formula.^{21,22} This strategy has been used for the round jet simulations discussed in Sec. III.

A criticism of EFLES may be that the method does not prescribe a cutoff wavenumber, or even a relation between cutoffs of the implied filtering of the numerical method and the explicit filter. In the overall process of obtaining an LES, this has not been a failing. Typically, all computations will begin with a level of discretization, and then, spectra and convergence of large scale quantities with refinement should be examined. If one is able to use a larger cutoff for filter E , the solution on a given grid may be better, but refinement can provide a significantly better result—evident in Sec. III, Fig. 4. So, determining an optimum cutoff, which would be universal, has not seemed to be a useful direction to pursue.

B. Functional modeling in EFLES and the spectral buffer

For simulations of unsteady, spatially developing flows, it is a widespread practice to have a buffer zone adjacent to, and immediately

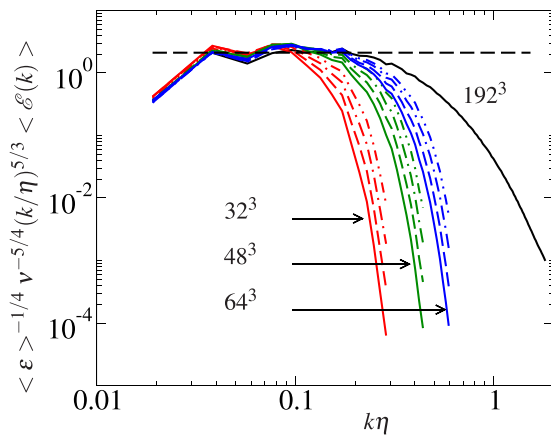


FIG. 4. Compensated energy spectrum from forced homogeneous, isotropic turbulence simulations of Chakravorty.¹⁸ LES grid sizes are 32^3 , 48^3 , and 64^3 , and DNS is with 192^3 points. For each group of LES, there are four curves corresponding to simulations with four filter cutoff values.

upstream of, the outflow boundary. Within the buffer zone, the solution will not have the same accuracy as that in the region of interest. It may even be quite wrong. In some treatments, the grid in the buffer zone is coarsened aggressively, and smaller scale motions that convect into the buffer zone become damped numerically because they can no longer be represented in coarse regions. Damping can also be effected by adding a term to the differential equations that takes the solution to a smoother profile. Then, at the outflow boundary, a simple convective condition with a uniform convection velocity, or the more detailed treatment based on characteristics^{23,24} can be applied. In such cases, there is an expectation that any significant error due to the buffer zone treatment will be restricted to the buffer zone, and to a smaller extent upstream of the buffer, to about the width of the outgoing shear layers.

There are two reasons why the effect of the buffer zone should not affect the upstream solution significantly. First, near such outflow regions, the flow is constantly convecting flow properties, including errors, out of the domain. For incompressible flow, pressure is obtained from a Poisson equation whose source terms are functions of the erroneous velocity field in the buffer zone; their effect on the solution, and the error, decays radially outward from such points.

Our studies with EFLES indicate that the result of filtering is analogous to using a buffer zone in spectral space. The spectral buffer spans a small range of the represented high wavenumbers ($k_{\text{cutoff}} < k < k_{\text{max}}$) and the corresponding range of represented high frequencies. Though the relatively small scale motions in this range are also computed, the filter E damps the energy contained in this range, smoothly and increasingly toward k_{max} . For all wavenumbers smaller than those of the spectral buffer, all spatial operations are performed with spectrally accurate schemes. The notion of a spectral buffer is suggested strongly by the shape of the filter response functions of the numerical schemes and the explicit filter. In all computations employing this approach, these functions have an essentially flat portion over a significant range of represented wavenumbers, and a smooth falloff beyond. For the two kinds of computations represented in Figs. 2 and 3, the spectral buffer spans the approximate range of $0.7 < k/k_{\text{max}} < 1$. In this range, the numerical schemes have significant errors. Errors in the

solution that would cause divergence begin to appear because the physical (and mathematical) requirement of energy transfer to smaller scales ($k > k_{\text{max}}$) and physical dissipation at these scales is not met in an LES. A spectral buffer is a range of scales that are computed and wherein energy is suppressed by filtering. The advantage over SGS models like the Smagorinsky is that in EFLES there is no suppression, or numerical dissipation over a range of low wavenumbers. Of course, physical dissipation over this range is simulated accurately. Just as one is not concerned about what happens within and beyond a physical buffer layer, one should not be concerned about what happens within and beyond the spectral buffer. However, all effects of the buffer zone on the low wavenumber content should be understood.

High resolution numerical methods and flat low-pass filters provide for a small spectral buffer—one that spans a small fraction of the computed scale range only. When low-order schemes are used, there is significant filtering even of low wavenumber content, making the method less efficient: then, a relatively finer grid would be needed for the same level of accuracy over a fixed range of large scales. This is the improved functional modeling provided by explicit filtering as an SGS model, though it was derived as a structural model.

The analogy between the spectral buffer of explicit filtering and physical outflow buffers provides a guideline for the shape of filter response function. Outflow buffer zone treatments are designed to suppress fluctuations so that simple boundary conditions applied to a smoothed flow prove to be effective. If the change is abrupt at the interface between the region of interest and the buffer, problems appear at the interface. Filter response functions of explicit filters used in all the cases cited here fall off smoothly near the high wavenumber end as in Figs. 1–3. If the explicit filter had a sharp cutoff at some $k_{\text{cutoff}} < k_{\text{max}}$, there would be energy accumulation near k_{cutoff} and the computations would diverge.

The term “spectral buffer” appears in Adams²⁵ as the range of represented scales that are not resolved by the numerical method. He explains that ADM was intended to “amplify scales in this buffer” and a “relaxation term was introduced as a dissipative mechanism on this buffer range.” So the term was used to label the range of scales where additional procedures were applied. In this paper, the term spectral buffer is used as an analog of outflow buffers in physical space, as a way to understand the functional modeling being effected, and not just as a name for a scale range where some procedures were to be applied.

1. Interscale energy transfer in EFLES

Sources of error in LES can be understood by dividing the energy spectrum of a turbulent flow into three wavenumber ranges with labels R: $k < k_I$; B: $k_I < k < k_R$ and U: $k > k_R$. k_R is the maximum wavenumber represented in the LES and is determined by the grid spacing. Wavenumbers larger than k_R are not represented in the computations. So “U” is the unrepresented range. Wavenumber k_I lies in the inertial range and corresponds to the lower of the cutoffs of the numerical method (implied filter) or explicit filter. When using a high-resolution scheme and filter, response functions are flat for smaller wavenumbers. So “R” is the resolved range, and “B” is the buffer range of wavenumbers that are represented in the computation, but where the solution is not computed correctly (unresolved).

For incompressible flow, the nonlinear terms in the Navier–Stokes equations are quadratic. So we should consider triad interactions between wavenumbers k_1 and k_2 giving rise to energy at

wavenumber $k_3 = k_1 \pm k_2$. Let the amplitudes of the interacting structures be A_R , A_B , and A_U to denote amplitudes in the three ranges. Owing to the energy cascade, $A_R > A_B > A_U$. Table I lists the different types of interactions when k_1 and k_2 are in the three ranges. All interactions that result in wavenumber k_3 in the resolved range are important. Cases 1 and 2 are computed correctly by EFLES. Cases 3, 5, 7, and 9 result in content in the buffer or unresolved range and will be suppressed by the filtering. Note also that due to the fall in the energy spectrum, the amplitudes of the resulting structures are small compared to what is computed correctly (cases 1 and 2). Case 4 can be a source of significant error when k_1 is small. Case 6 results in smaller errors when the amplitude in the buffer range is small compared to the peak amplitude in the resolved range. Cases 8 and 10 imply errors in the resolved range from interactions that are not accounted for, but may be neglected due to the small amplitudes of the interacting pairs. This is a guideline for estimating the extent of the error due to the unrepresented range from the solution spectra. A conservative upper bound would be case 6, which is an erroneous underestimate of the contribution from buffer scale interactions on the large scales. This is the most significant backscatter error in this method. Of course, backscatter from wavenumbers in the resolved range (case 2) is captured correctly. As a general guideline, the cutoff wavenumber needs to be large enough so that the effect of small scales on the dynamics of the large scales is no longer significant, hence the need for judicious grid refinement. Implicit in the discussion above is the model energy spectrum, which has a peak at some small wavenumber, a $k^{-5/3}$ fall through the inertial range and a rapid falloff near the Kolmogorov scale. In nearwall regions, the solution is dependent on the dynamics of thin elongated structures—the alternating streaks—which have widths and spacing that scale on wall units. Thus, the backscatter from their interactions to larger scales is important, and grids spacing must be small enough to resolve these interactions. Thus, the spacing in wall-normal and spanwise directions in LES is comparable to those for a DNS, in the nearwall region.

The discussion of interscale interactions provides a further connection to a physical buffer. The turbulence energy cascade implies a net transfer of energy from large scales to small scales, like convection to a physical outflow buffer. If the spectral buffer is at suitably large enough wavenumbers, the incorrect backscatter may be ignored because the amplitudes are relatively small. The response function of

TABLE I. Interscale interactions. “+” and “-” in column 1 denote sum and difference interactions, respectively.

Case	Type	k_1	k_2	k_3	Amplitude of k_3	Effect on LES
1	+	R	R	R, B, U	$A_R A_R$	Important
2	-	R	R	R	$A_R A_R$	Important
3	+	R	B	B, U	$A_R A_B$	Unimportant
4	-	R	B	R	$A_R A_B$	Important
5	+	B	B	B, U	$A_B A_B$	Unimportant
6	-	B	B	R	$A_B A_B$	Important
7	+	B	U	U	$A_B A_U$	Unimportant
8	-	B	U	R, B	$A_B A_U$	Important
9	+	U	U	U	$A_U A_U$	Unimportant
10	-	U	U	R, B	$A_U A_U$	Important

the explicit filter vanishes at k_{\max} analogous to a nonreflecting outflow boundary condition at the end of the physical buffer.

III. LES EXAMPLES

When there is a clear separation between cutoff wavenumbers of the numerical scheme and the explicit filter, it is possible to examine the effect of changing the cutoff wavenumber of the explicit filter alone. With LES of supersonic channel flow, Mathew *et al.*² had shown *monotonic* convergence toward the DNS solution as the LES grid was refined, or as filter cutoff was increased. An even more compelling demonstration was obtained by Chakravorty¹⁸ by performing several LES and a DNS of forced homogeneous, isotropic turbulence. Figure 4 shows the compensated energy spectrum as a function of wavenumber k scaled with the Kolmogorov length scale η . The DNS was on a grid of $192 \times 192 \times 192$ points, and the Taylor Reynolds number was about 80. LES was conducted on grids of 32^3 , 48^3 , and 64^3 points, with four different values of cutoff wavenumbers of the explicit filter. Clearly, (a) LES solutions converge monotonically to the DNS with grid refinement and toward DNS when the filter cutoff is increased on a given grid, and (b) the changes are to high wavenumber content only. As the grid size increases, there is essentially no change to low wavenumber content even as the spectral range increases. If one compares the DNS with any one of the LES, say, on the 32^3 grid and with the smallest filter cutoff wavenumber, one infers that explicit filtering provides a spectral buffer beyond scaled wavelength $k\eta \approx 0.1$ (η is the Kolmogorov length scale). The falloff of the spectrum is due to the filter since the numerical differentiation is spectrally accurate over a larger range. On a given grid, as the filter cutoff wavenumber is increased, the spectral buffer zone becomes thinner. Solutions on different grids demonstrate a complementary feature: on a finer grid, the buffer zone has moved to a range of larger wavenumbers. Significant errors remain confined to this buffer zone. While it not *a priori* evident that errors would be confined to wavenumbers larger than the scheme cutoff, these results show no significant contamination of smaller wavenumber content.

The results from forced, homogeneous, isotropic turbulence simulations of Patel²⁶ on larger grids are shown in Fig. 5. Taylor Reynolds number was 108. The same conclusions apply: As the grid is refined and the spectral range increases, the range of wavenumbers over which

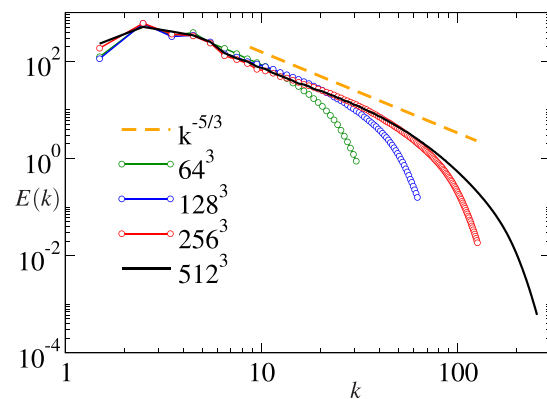


FIG. 5. Energy spectrum from forced homogeneous, isotropic turbulence simulations of Patel.²⁶ Simulations in cubes of size $2\pi^3$ spanned by 64 – 512 gridpoints in each direction.

an inertial range occurs increases with little change to the content at lower wavenumbers. Solutions tend almost monotonically to the DNS (512^3 box) as the grid is refined. The spectra fall off rapidly in a buffer range of wavenumbers.

A second example is that of spatially developing, compressible round jets at very high Reynolds numbers. Simulation parameters are listed in Table II. The Reynolds number $Re = U_0 D / \nu$ is based on jet diameter D and its centerline velocity U_0 at the nozzle exit plane. Inflow plane Mach number M is 0.9. A near top-hat velocity profile with a tanh bounding shear layer was specified at the inflow plane. Small-amplitude, random fluctuations were imposed on the shear layer alone. Simulations A and B are at $Re = 11\,000$, but for different domain sizes—axial distances of $30D$ and $70D$, with approximately the same grid spacing. Bogey and Bailly¹³ have simulated a round jet for $75D$ at these conditions ($Re = 11\,000$ and $M = 0.9$). Cases C and D are at the much higher Reynolds number of 1.1×10^6 . Spatial differences were obtained with a sixth-order compact scheme, and a tenth-order filter was applied to conserved variables after every time step. Filter response functions are those in Fig. 3. Time-stepping is with a second-order, explicit, Runge–Kutta scheme. Nonreflecting boundary conditions²⁴ were applied at the downstream and lateral boundary surfaces. The numerical method has been discussed elsewhere,²² and the details of the solution are in Patel.²⁶

The Cartesian reference frame used is shown in Fig. 6; the x -axis was aligned with the jet, and the origin is at the center of the jet on the inflow plane. The domain of interest is $0 < x < L_x$, $-L_y/2 < y < L_y/2$, $-L_z/2 < z < L_z/2$. The numbers of gridpoints in this region are also given in Table II. Within this region, the grids were stretched in lateral directions outside a central square of side $1.5D$; grid spacing was increased in geometric progression by 1%. For cases B and D, the grid was stretched axially as well at 0.7%. The actual computational region was larger because physical buffer zones were used near the downstream and lateral boundaries where the grid was stretched aggressively at 10%. The additional gridpoints in these buffer zones were 30 in the axial and 20 in the lateral directions. Fine scale structures disappear in the buffer zone as they cannot be represented on the coarser grid.

An impression of the scale range is conveyed by iso-surfaces of vorticity magnitude from cases A and D in Fig. 6. The larger scale range at the higher Reynolds number is evident. A sensitive test of the correctness of these solutions is the development of the inverse of the centerline velocity and the level of velocity fluctuations. The inverse of the centerline velocity $U_c(x)$ is shown in Fig. 7. For clarity, the curves for cases C and D have been offset upward by three units. The change in slope at $x/D \approx 10$ is the beginning of the turbulent portion. In all cases, there is a clear linear range following breakdown. The curved portion near the downstream end is from the outflow buffer region.

TABLE II. Round jet simulation parameters. $L_z = L_y$ and $N_z = N_y$.

Case	Re	L_x/D	L_y/D	N_x	N_y	B_u
A	1.1×10^4	30	10	263	253	6.01
B	1.1×10^4	70	40	426	473	5.92
C	1.1×10^6	30	10	263	253	7.04
D	1.1×10^6	30	10	406	387	6.03

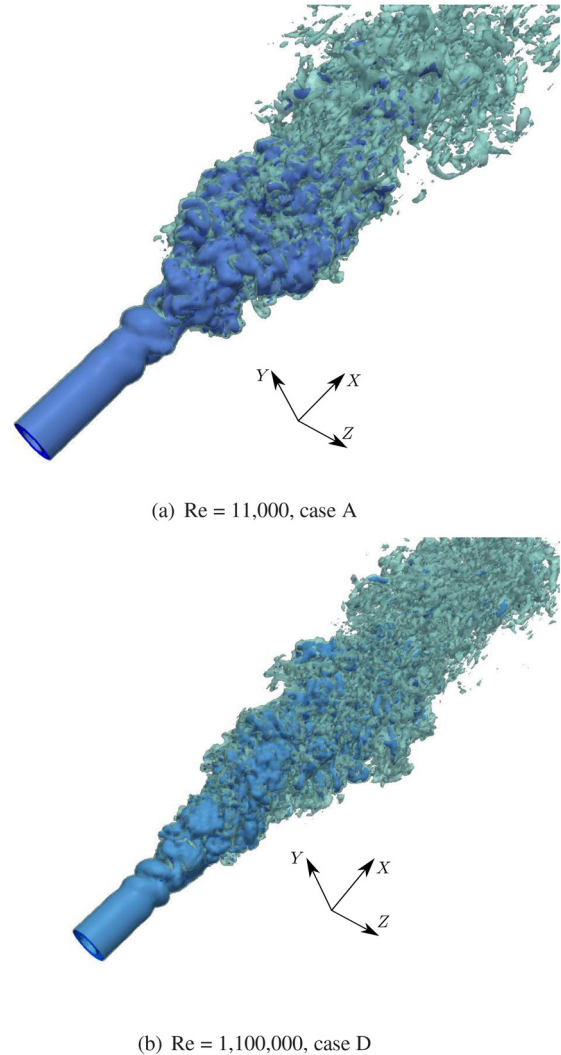


FIG. 6. Iso-surfaces of vorticity magnitude $\omega D / U_0 = 7.8, 15.6$.

Comparing cases A and B, we observe that when the simulation domain was extended, the slopes of these curves remained essentially the same. Linear fits for case B over the portion $10 < x/D < 60$ and over $10 < x/D < 30$ for case D have been included. The reciprocal of the slope of the linear fits, B_u , is listed in Table II. The values for cases A and B are close to each other and agree closely with values from experiments (5.8–6.06; Table 5.1 in Pope²⁷). Incidentally, the curves for cases A and B also illustrate the correct effect of using a physical buffer layer: Only within its buffer layer does the solution for case A depart from the solution for case B. For the coarse grid case C, we do not obtain a linear variation, but one which curves slightly. The grid and domain were identical to those for case A. With a fourfold increase in the number of gridpoints for case D, we recover a linear variation and slope parameter $B_u = 6.03$ in the correct range. A small increase in the number of gridpoints sufficed for a 100-fold increase in the Reynolds number because this is an LES.

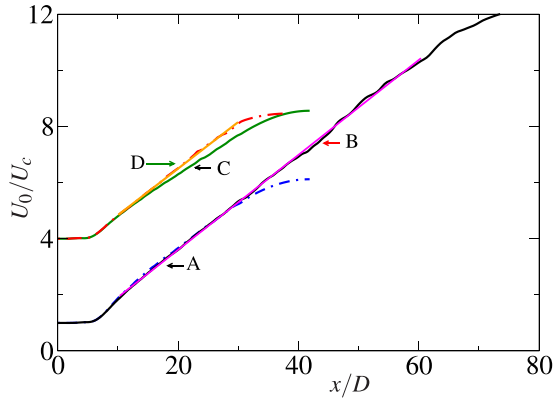


FIG. 7. Centerline mean velocity U_0/U_c . Curves for cases C and D have been vertically offset by 3 units for clarity. Case A (blue filled circle with dashed line), case B (—), case C (green long-dashed line), and case D (orange filled circle with dashed line). Linear fit over turbulent region for case B (pink long-dashed line) and for case D (orange long-dashed line).

Figure 8 shows the development of velocity fluctuations along the centerline, scaled with the local centerline mean velocity. For cases A, B, and D, the axial component u_{rms}/U_c tends to 0.24, as in experiments.^{28,29} Fluctuation levels are smaller for the coarse grid case C and is consistent with the weaker decay rate of the centerline velocity (Fig. 7). The grid employed for case C is inadequate, but on refinement (case D), an acceptable LES has been obtained. Also, as in experiment, both cross-stream components v_{rms}/U_c and w_{rms}/U_c were found to tend to 0.18 (not shown here).

Time series of velocity components at many stations on lines $y = 0, z = 0$ (jet centerline) and $y = D/2, z = 0$ (jet boundary shear layer at inflow plane) were stored. Frequency spectra were calculated using the PWELCH function in MATLAB 8.6. Figure 9 shows the frequency spectra of the streamwise velocity component, scaled with the local mean centerline velocity, $E(u)/U_c^2$, at $x/D = 4.99, 7.45, 9.96, 12.56,$ and 14.94 from case A. Frequency f has been scaled with the jet half-radius $r_{1/2}$ and U_c . Close to the inflow plane, the spectral range is small and solution field is fully represented and accurately computed on the

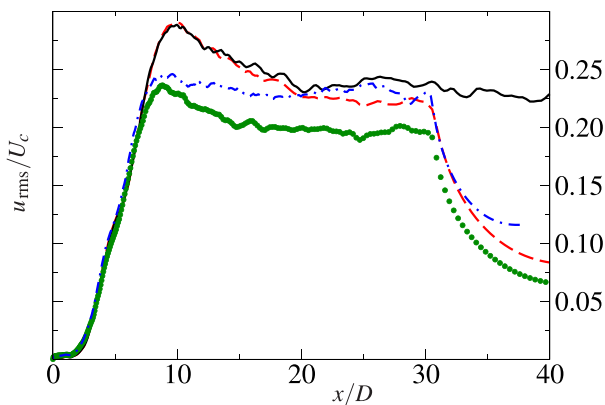


FIG. 8. Centerline velocity fluctuations. u_{rms}/U_c : case A (blue filled circle with dashed line), B (—), C (green filled circle), and D (orange dashed line).

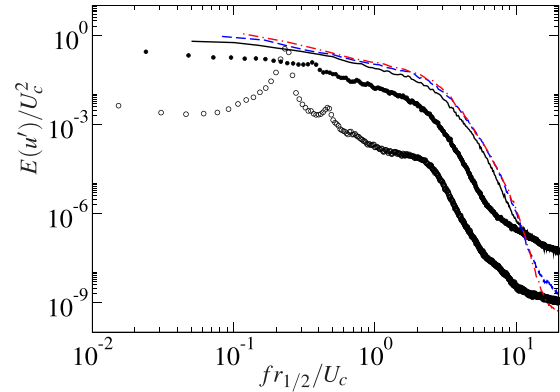


FIG. 9. Scaled power spectra, case A. $x/D = 4.99$ (\circ), 7.45 (\bullet), 9.96 (—), 12.56 (blue dashed line), and 14.94 (orange dotted-dashed line).

chosen grid. Regular oscillations due to the vortex rings upstream of breakdown (see Fig. 6) can be observed as a low frequency peak in the spectrum at $x/D = 4.99$. Downstream, this peak disappears as the flow breaks down to turbulence, and the spectrum broadens. Spectra collapse on these local scales to show self-preserving development for $x/D \geq 9.96$.

Figure 10 shows spectra from cases A, C, and D at $x/D \approx 12$. When the Reynolds number alone is changed, the spectra should extend to smaller frequencies as the inertial range extends, while the content at low frequencies should remain approximately the same (cases A and D). Clearly, the simulations support this expectation. When the grid is refined, the spectrum extends as smaller lengths and frequencies can be represented and computed accurately (cases C and D). Again, the changes are to the high frequency end of the spectrum, while the low frequency part of the solutions remains essentially the same.

Recall the discussion of interscale interactions in Sec. II B 1: Interaction cases 4 and 6 that contribute to large scale content can be in error if the spectral range of the buffer begins at too small a wavenumber. Power spectra from cases A, C, and D in Fig. 10 show that a small shift to higher wavenumbers of the spectral buffer sufficed to obtain a solution with slope parameter in the correct range.

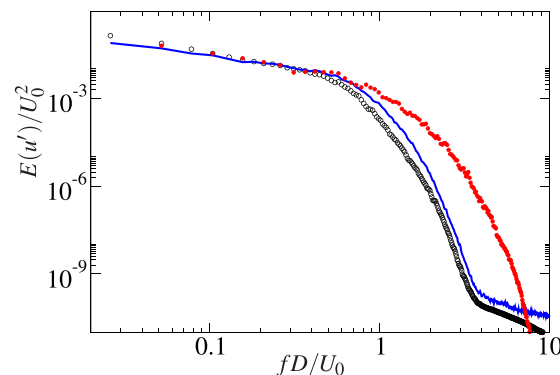


FIG. 10. Power spectra at $x/D \approx 12$. Case A (\circ), case C (blue long-dashed line), and case D (red filled circle).

IV. OTHER SGS MODELS

With this understanding, we can consider SGS models.

The Smagorinsky SGS model is implemented as a term added to the momentum equations by setting the SGS stress tensor,

$$\tau_{ij}^{sgs} = \nu^{sgs} S_{ij},$$

where S_{ij} is the strain rate tensor and ν^{sgs} is the eddy viscosity. The effect of this term is to damp *all* scales. Briefly, consider the 1-d Eq. (3) for the “LES” variable \bar{u} . A Smagorinsky-type model for \mathcal{R} would appear as

$$\frac{\partial \bar{u}}{\partial t} + \frac{\partial}{\partial x} f(\bar{u}) = \nu^{sgs} \frac{\partial^2 \bar{u}}{\partial x^2}. \quad (9)$$

Here, for ease of illustration, let ν^{sgs} be a constant, though in the Smagorinsky model, it is proportional to a measure of the local strain rate tensor. On taking the Fourier transform of Eq. (9), and Euler forward time-stepping, we can write

$$\hat{u}(k, t + \Delta t) = \hat{u}(k, t) - \Delta t(ik\hat{f}) - \Delta t \nu^{sgs} k^2 \hat{u}(k, t).$$

Combining the first and third terms on the right hand side shows that the integration is equivalent to applying a filter with response function $\hat{G}_S = 1 - \Delta t \nu^{sgs} k^2$ to the solution at t before time-stepping. This filtering provides the SGS modeling. Although high wavenumber content is damped more (increases as k^2), *all* content is damped. This is not to be considered a wrong model, because the damping of any fixed range of low wavenumber content will reduce as the grid is refined, but is, therefore, a less efficient model.

An earlier method called MILES had also been characterized as an implicit large eddy simulation (ILES). Boris³⁰ had explained the effectiveness of MILES by stating, “monotone convection algorithms designed for positivity and causality, in effect have a minimal LES filter and matching subgrid model already built in. [This ensures] efficient transfer of the residual subgrid motions, [...] off the resolved grid with minimal contamination of the well-resolved scales by the numerical filter.” These features turn out to be requirements that appear in the derivation of EFLES. A variety of experiences with MILES, including a historical account, was discussed by Grinstein *et al.*³¹ One way to understand the success of MILES is to recall that in the flux-corrected-transport (FCT) algorithm, the anti-diffusive step is constructed from the local solution, and limited, to ensure that no new extrema are created. The FCT algorithm was designed to obtain higher-order flow fields, capturing shocks without oscillations. It proves effective as an algorithm for LES because it suppresses oscillations that will appear as nonlinear terms generate content at wavenumbers larger than the ones that can be represented on the chosen grid. In its treatment of the difficulty at the high wavenumber end, the algorithm is also optimal because it is designed to just prevent the appearance of new extrema based on the local state. Away from locations where the integration would not produce a new extremum, there is no modification of the solution. The implied filter is then active in a high wavenumber spectral buffer. Since MILES was found to be useful for LES without any explicit SGS model terms, the basic numerical method remained of relatively low order—FCT is second-order in space. On discovering that a compact scheme with a high-order filter delivers useful LES without adding SGS model terms, Visbal *et al.*³² have termed their method an ILES also. The explicit filtering methods cited here no longer attempt

to provide any kind of dynamic, optimal filtering. Attempts in this direction did not reveal any significant benefit by changing the filter cutoff, or by reducing the frequency of its application.

A. Secondary filtering

Adams³³ had added a low-order relaxation regularization term to the differential equation for the LES field. In Stolz and Adams,⁴ this was briefly mentioned as the use of a secondary filter that improved the solution, but results were not included pending further investigation. It has been added and discussed in detail subsequently.^{6,34} When this term is added, the model Eq. (5) would be modified to read

$$\frac{\partial \bar{u}}{\partial t} + G * \frac{\partial f(Q * \bar{u})}{\partial x} = -\chi(I - Q * G) * \bar{u}. \quad (10)$$

Here, χ is a free parameter. Stolz *et al.*⁶ found solutions to have but a weak dependence on χ . Mean velocity profiles showed very little difference as χ was changed by a factor of 8. As stated in Stolz *et al.*,⁶ the effect of adding this relaxation term can be realized by integrating without the additional term and filtering the field \bar{u} with filter QG every $1/(\chi\Delta t)$ timesteps. Or, that applying the filter QG to field \bar{u} every m timesteps while integrating Eq. (5) is equivalent to integrating Eq. (10) with $\chi = 1/(m\Delta t)$. If $m = 1$, relaxation regularization is realized by applying the resultant filter $E^*E = G^*Q^*G^*Q$ to the evolving field. For flat filters of the type shown in Figs. 1 or 2, $E(\alpha_1) * E(\alpha_1)$ can be approximated by applying filter $E(\alpha_2)$, with α_2 slightly less than α_1 . So, a formal secondary filtering step is not indicated since the distinguishable benefit that would accrue is not evident.

V. CONCLUSIONS

The explicit filtering method for LES comprises integration of the governing transport equations without any added SGS terms, and the application of a flat low-pass filter to the transported fields after every integration step. The effective spatial filtering of several such LES, including the filtering implied by the spatial operations of the numerical schemes, was examined. A common feature of these implementations is a spectral buffer over a small part of the high wavenumber end of the range of represented scales, analogous to buffer or sponge zones near outflow boundaries. Since there is essentially no filtering of a range of large scales, and, as expected for LES, the smallest represented scales are in the inertial range where the amplitudes are small, when the scale range is increased, solutions converge monotonically to the full spectrum (DNS), *without* any significant changes to the large scale parts. The monotonic convergence of gross quantities (means and low order moments) is a consequence of adding content at the high wavenumber end only when the grid is refined. Any LES should converge to the DNS with grid refinement, but monotonic convergence allows one to use an LES from modest-sized grids with the expectation that it is qualitatively correct, and that grid refinement will provide quantitative improvements. Although it is not surprising that the *procedure* has been seen as an example of an implicit LES (ILES), as a clean-up operation, or, as a numerical operation to suppress (undefined) instabilities, it ought to be clear from the discussion above that the explicit filtering method provides an SGS model for obtaining an LES. The principle revealed herein is quite general and can be used to understand the observed or potential effectiveness of other methods for LES as well.

ACKNOWLEDGMENTS

I have learned much from the published work and presentations of Professor K. R. Sreenivasan and consider it a privilege to have this paper included as a tribute to him. I thank my students Dr. S. Chakravorty and Dr. Sumit Patel who provided data from their simulations for the discussions in Sec. III. I thank my colleague Professor Santosh Hemchandra for useful, critical discussions on EFLES. His experience from applying EFLES to several other more complex flows has provided us with further confidence in this approach to LES.

AUTHOR DECLARATIONS

Conflict of Interest

The author has no conflicts to disclose.

Author Contributions

Joseph Mathew: Conceptualization (equal); Writing – original draft (equal); Writing – review & editing (equal).

DATA AVAILABILITY

The data that support the findings of this study are available within the article.

REFERENCES

- ¹P. Sagaut, *Large Eddy Simulation for Incompressible Flows*, 3rd ed. (Springer, 2006).
- ²J. Mathew, R. Lechner, H. Foysi, J. Sesterhenn, and R. Friedrich, “An explicit filtering method for large eddy simulation of compressible flows,” *Phys. Fluids* **15**, 2279–2289 (2003).
- ³T. S. Lund, “The use of explicit filters in large eddy simulation,” *Comput. Math. Appl.* **46**, 603–616 (2003).
- ⁴S. Stolz and N. A. Adams, “An approximate deconvolution procedure for large-eddy simulation,” *Phys. Fluids* **11**, 1699–1701 (1999).
- ⁵ $\alpha = -0.2$ in Ref. 33, $\alpha = 0.25$ in Ref. 4.
- ⁶S. Stolz, N. A. Adams, and L. Kleiser, “An approximate deconvolution model for large-eddy simulation with application to incompressible wall-bounded flows,” *Phys. Fluids* **13**, 997–1015 (2001).
- ⁷B. J. Geurts, “Inverse modeling for large-eddy simulation,” *Phys. Fluids* **9**, 3585 (1997).
- ⁸J. A. Domaradzki and E. M. Saiki, “A subgrid-scale model based on estimation of unresolved scales of turbulence,” *Phys. Fluids* **9**, 2148 (1997).
- ⁹M. Germano, U. Piomelli, P. Moin, and W. H. Cabot, “A dynamic subgrid-scale eddy viscosity model,” *Phys. Fluids* **3**(7), 1760–1771 (1991).
- ¹⁰M. R. Visbal and D. V. Gaitonde, “High-order-accurate methods for complex unsteady subsonic flows,” *AIAA J.* **37**, 1231–1239 (1999).
- ¹¹M. R. Visbal and D. P. Rizzetta, “Large-eddy simulation on curvilinear grids using compact differencing and filtering schemes,” *ASME J. Fluids Eng.* **124**, 836 (2002).
- ¹²D. P. Rizzetta, M. R. Visbal, and P. E. Morgan, “A high-order compact finite-difference scheme for large-eddy simulation of active flow control,” *Prog. Aerosp. Sci.* **44**, 397–426 (2008).
- ¹³C. Boge and C. Bailly, “A family of low dispersive and low dissipative explicit schemes for flow and noise computations,” *J. Comput. Phys.* **194**, 194–214 (2004).
- ¹⁴D. Marinc and H. Foysi, “Investigation of a continuous adjoint-based optimization procedure for aeroacoustic control of plane jets,” *Int. J. Heat Fluid Flow* **38**, 200–212 (2012).
- ¹⁵C. Schaupp, R. Friedrich, and H. Foysi, “Transverse injection of a plane-reacting jet into compressible turbulent channel flow,” *J. Turbul.* **13**, N24 (2012).
- ¹⁶H. Foysi and S. Sarkar, “The compressible mixing layer: An LES study,” *Theor. Comput. Fluid Dyn.* **24**, 565 (2010).
- ¹⁷S. K. Lele, “Compact finite difference schemes with spectral-like resolution,” *J. Comput. Phys.* **103**, 16–42 (1992).
- ¹⁸S. Chakravorty, “On large eddy simulation of reacting flows using the explicit filtering method with a filtered mass density function,” Ph.D. thesis (Department of Aerospace Engineering, Indian Institute of Science, 2010).
- ¹⁹S. Chakravorty and J. Mathew, “A high-resolution scheme for low Mach number flows,” *Int. J. Numer. Methods Fluids* **46**, 245–261 (2004).
- ²⁰J. Mathew, H. Foysi, and R. Friedrich, “A new approach to LES based on explicit filtering,” *Int. J. Heat Fluid Flow* **27**, 594–602 (2006).
- ²¹S. Ganesh, “Flow and sound field of free and impinging jets from LES using explicit filtering method,” Ph.D. thesis (Department of Aerospace Engineering, Indian Institute of Science, 2013).
- ²²S. K. Patel and J. Mathew, “Large eddy simulation of supersonic impinging jets by adaptive, explicit filtering,” AIAA Paper No. 2015-2298 (2015).
- ²³K. W. Thompson, “Time dependent boundary conditions for hyperbolic systems,” *J. Comput. Phys.* **68**, 1–24 (1987).
- ²⁴T. Poinsot and S. K. Lele, “Boundary conditions for direct simulation of viscous flows,” *J. Comput. Phys.* **101**, 104–129 (1992).
- ²⁵N. A. Adams, “A stochastic extension of the approximate deconvolution model,” *Phys. Fluids* **23**, 055103 (2011).
- ²⁶S. K. Patel, “Aeroacoustics of supersonic jets impinging on wedge deflectors from LES,” Ph.D. thesis (Department of Aerospace Engineering, Indian Institute of Science, 2018).
- ²⁷S. B. Pope, *Turbulent Flows* (Cambridge University, 2000).
- ²⁸N. R. Panchapakesan and J. L. Lumley, “Turbulence measurements in axisymmetric jets of air and Helium. Part 1. Air jet,” *J. Fluid Mech.* **246**, 197–223 (1993).
- ²⁹H. J. Hussein, S. P. Capp, and W. K. George, “Velocity measurements in a high-Reynolds-number, momentum-conserving, axisymmetric, turbulent-jet,” *J. Fluid Mech.* **258**, 31–75 (1994).
- ³⁰J. P. Boris, “On large eddy simulation using subgrid turbulence models,” in *Whither Turbulence? Turbulence at the Crossroads*, edited by J. L. Lumley (Springer, 1990).
- ³¹*Implicit Large Eddy Simulation*, edited by F. F. Grinstein, L. G. Margolin, and W. J. Rider (Cambridge University, 2007).
- ³²M. R. Visbal, P. E. Morgan, and D. P. Rizzetta, “An implicit LES approach based on high-order compact differencing and filtering schemes,” AIAA Paper No. 2003-4098, 2003.
- ³³N. A. Adams, “Advances in direct deconvolution modeling of subgrid-scales for flows with discontinuities,” in *CTR Annual Research Briefs 1999* (Stanford University, 1999), pp. 317–327.
- ³⁴S. Stolz, N. A. Adams, and L. Kleiser, “The approximate deconvolution model for large-eddy simulation of compressible flows and its application to shock-turbulent-boundary-layer interaction,” *Phys. Fluids* **13**, 2985–3001 (2001).